STRESS AND BUCKLING ANALYSIS OF A DOUBLE-BUBBLE TANK STRUCTURE

By

James C. Robinson
NASA Langley Research Center

and

John H. Dutton
McDonnell Douglas Corporation

SUMMARY

An analytical study of a two-lobed circular arc pressure vessel (double-bubble tank) with a local perturbation from the cylindrical shape has been made. From this study, it can be concluded that NASTRAN provides a good linear buckling analysis capability for structures that cannot be handled by other analysis techniques. However, at the present time, solutions are relatively expensive from a computational standpoint. Two worthwhile additions to the NASTRAN program would be the inclusion of a new beam element that adequately represents the shear transfer when modeling stiffeners on a shell and the capability, in a rigid format, to keep certain prescribed loads constant during the eigenvalue extraction process.

INTRODUCTION

Some space shuttle orbiter configurations considered in the early stages of the Phase B studies had a two-lobed intersecting circular arc (double-bubble) pressure vessel for cryogenic propellant storage. In the orbiter configuration shown in figure 1, the tank was integrated into the orbiter as part of the primary fuselage structure and, therefore, was subjected to overall structural loads, such as axial compression, in addition to the loads induced by internal pressure. The fabrication method selected for the tank required that sections of the tank approximately 3.0 m (10 ft) in length be joined by full circumferential welds. Automatic welding was selected as the method to provide the weld quality required, but automatic welding equipment would not function satisfactorily in the cusp formed by the intersection of the two cylinders. Therefore, a local perturbation from the double-bubble shape was required to provide an acceptable radius on the

shell wall, as shown in figure 2.

The selection of an analysis method for the problem was limited by the complexity of the structure. The lack of axisymmetry precluded the use of shell-of-revolution programs for other than preliminary studies of modeling requirements and the existing form of a general shell program, STAGS, (ref. 1) was incapable of analyzing the shell with the perturbed shape. Thus, recourse to a finite element technique was required for detailed analysis.

The purpose of this paper is to present the results of a study using NASTRAN to determine the effect of the shape perturbation on the stress distribution and axial buckling load of the tank. A secondary purpose is to present some observations based on experience gained during the study in the use of NASTRAN for shell analyses.

PRELIMINARY STUDIES

Shell-of-Revolution Study

A preliminary study of a ring- and integral-stringer stiffened cylindrical shell having the same diameter and stiffener dimensions as one lobe of the tank was made using the shell-of-revolution analysis of reference 2 to gain some insight into modeling requirements for the tank analysis. Simply supported cylinders with a length equal to (1) a complete lobe between end domes, and (2) one bay of a lobe between tank rings were analyzed for a loading consisting of positive internal lateral pressure and net axial compressive loads. The results of this study (fig. 3) are that the longer cylinder (with rings and stringers considered distributed) buckles axisymmetrically and hence is independent of the ratio of the hoop stress resultant/axial stress resultant (N_y/N_x). The buckling mode half-wave length of 23.0 cm (9.1 in.) approximates half the bay length between rings. The shorter cylinder buckles asymmetrically for small negative values of N_y/N_x, but approaches the analytical buckling load of the longer cylinder and buckles axisymmetrically with a half-wave length of 25.4 cm (10.0 in.) for values of N_y/N_x less than about -1.0. These results and the details of the tank geometry, stiffness, and loads ($N_y/N_x < -1$ for the stiffened area of the tank) suggest that a satisfactory approximation to the complete double-bubble tank could be obtained by limiting the model to one-half of one bay longitudinally and about twice that distance circumferentially to give a model covering an area of 25.4 by 55.4 cm (10 by 21.8 in.) (fig. 2a). The effect of the remainder of the structure was included by the use of assumed boundary conditions.

Modeling Detail Studies

Several short studies were conducted to evaluate the effects of modeling details on the NASTRAN results. In one study, the effect of radius to thickness ratio (R/t) on the axisymmetric buckling load of an unstiffened

cylinder was calculated using NASTRAN with a model composed completely of quadrilateral elements (CQUAD2). For dimensions similar to the NASTRAN demonstration problem ($R/_t$ of 32, ref. 3), the buckling load was 1.4 percent above the classical buckling load and the buckling mode shape was the classical shape of two longitudinal half-waves. As $R/_t$ was increased for a model containing the same number of elements (by decreasing the shell thickness), the discrepancy between buckling loads calculated with NASTRAN and those obtained from classical theory increased to 6.8 percent at $R/_t$ of 320. In addition, the NASTRAN analysis predicted a mode shape with six half-waves compared to seven for the classical solution. The increase in the number of half-waves with an increase in $R/_t$ requires more severe element deformation and is probably the cause for the increased discrepancy. These results suggest that for axisymmetric buckling problems, the number of elements per half-wave should be greater than the value of 3.3 obtained in the reduced thickness demonstration problem ($R/_t$ = 320).

Another modeling detail study was designed to check the modeling of the longitudinally stiffened area of the tank. A stiffened circular cylinder of the same dimensions as one bay of the tank loaded by internal pressure and axial forces was analyzed using NASTRAN. BAR elements with bending stiffness were used in modeling the stiffeners to obtain the proper combination of axial and bending stiffness and adequate detail of stress output. However, modeling of a longitudinal stiffener as an offset BAR element produced unreasonable discrepancies in the stresses in adjacent elements when radial expansion of the end of the cylinder was prevented either by a ring or by radial displacement boundary conditions. A quadrilateral shear panel between the beam element and the shell was used to improve the model. Figure 4 shows the stresses due to a static loading in a longitudinal stiffener with and without the quadrilateral shear panels in the model. The smaller discontinuities in the calculated bending stresses using the model with the quadrilateral shear panels indicate that it is the better representation of the actual structure. The difference in stresses results from the mechanism of shear transfer in the composite section (stiffener and shell) and is similar to the problem discussed previously in reference 4. The inclusion in NASTRAN of the shear beam element discussed in reference 4, or an element with similar properties, should improve the NASTRAN modeling capability for this type of structure.

The axisymmetric buckling load for the cylinder discussed above, with the same boundary conditions as used in reference 2, was calculated using NASTRAN. This buckling load was about 2 percent higher than that given by the shell analysis of reference 2 and the buckling mode shape which had two half-waves was the same as that given by the shell analysis. It would appear, therefore, that the addition of longitudinal stiffeners to the relatively thin shell with an $R/_t$ of 1277 increases the local moment of inertia sufficiently to force a longer wave length for the buckling mode shape of the stiffened shell (10 elements per half-wave) and thus provides

satisfactory correlation between buckling predictions made with the use of classical theory and NASTRAN.

In the final modeling detail study, the validity of representing a complete cylinder by use of a single bay of that cylinder with assumed boundary conditions to simulate the remainder of the cylinder was evaluated by comparing the axisymmetric buckling load for a complete multi-bay cylinder with that for a single bay cylinder with assumed boundary conditions. NASTRAN was used to calculate the axisymmetric buckling load and mode shape of a complete five-bay cylinder. The cylinder selected (fig. 5) had relatively light rings and shorter end bays with rotationally restrained ends to insure buckling in the center portion. The loads were internal lateral pressure and enforced axial displacement. For the buckling calculation, the axial restraint was removed by the use of an ALTER package provided the NASTRAN Systems Management Office by Malcolm W. Ice of Boeing Computer Sciences, Inc. The buckling load for the five-bay cylinder was essentially the same as for the single bay cylinder and the buckling mode shape (fig. 5) is antisymmetric about the centerline, but the node locations do not occur at the frames. This may be due to the small frame extensional stiffness which is only about 12 percent of the shell extensional stiffness in the hoop direction. This agreement in the axisymmetric buckling loads for the two cylinders indicates that the use of assumed boundary conditions is satisfactory even with the use of light rings which do not force nodes to occur at the rings.

DOUBLE-BUBBLE TANK STUDY

Model and Loads

The tank was analyzed both with and without the shape perturbation to determine its effect on deflections, stresses, and buckling loads. The part of the double-bubble tank that was modeled is shown in figure 2, and the finite element model, a contour plot of the shape perturbation, and the shell thickness are shown in figure 6. The cylindrical portions of the shell were modeled with flat quadrilateral elements having membrane and bending properties (CQUAD2). The transition section of the perturbation was modeled with triangular elements having similar properties (CTRIA2). The integral longitudinal stiffeners were modeled as offset BAR elements with quadrilateral shear panels to provide a better approximation of the local shear transfer mechanism as determined in the preliminary studies (see fig. 4). The frame section was composed of rod elements and quadrilateral and triangular membrane elements. The frame was considered to elastically restrain the tank in the plane of the frame, but buckling of the frame was prevented by the imposition of deflection constraints normal to the plane of the frame.

To simulate the effect of the remainder of the structure on the portion of the tank that was modeled, appropriate restraint conditions were assumed for the boundaries of the model. Symmetric boundary conditions were assumed along the centerline of the double-bubble tank for both the prestress (static) and buckling computations. Symmetric boundary conditions were assumed along

the outer edge parallel to the tank centerline for both prestress and buckling computations. On the boundaries at the frame and along the bay centerline, zero rotation in the circumferential direction was assumed for the prestress calculations. For buckling, four combinations of symmetric and antisymmetric restraints were used to insure that the minimum value of the buckling load was obtained.

The loads imposed for prestress on the double-bubble tank resulted from a positive internal pressure of 207 $kN/_m2$ (30.0 psi) and an enforced axial displacement of 0.051 cm (0.020 in.), which corresponds to a strain of 0.002. The enforced displacement was used to simulate overall compression of a structure of variable thickness at a distant location from the ends of the structure. This combination of loads produces a stress resultant ratio N_y/N_x of approximately -1.1. NASTRAN rigid format 5 requires that this ratio remain constant during buckling. Inasmuch as the tank internal pressure and the applied axial load are not physically coupled, it would have been desirable to have the option of letting only one stress resultant vary during buckling.

Numerical Results

The results of the NASTRAN calculations for the double-bubble tank both with and without the shape perturbation are shown in figures 7 through 10. All of these figures are nondimensionalized contour plots, where the contours are lines of constant percentage of the maximum value (shown in the subtitle) of the functions shown in the figure title. In all figures, plot (a) presents values for the tank without the shape perturbation, and plot (b) presents values for the tank with the perturbation. The plots were drawn by a computer program that is a modification of the contour plot program described in reference 5.

Comparison of the contour plots for the radial displacement of the tank without and with the perturbation (fig. 7) shows similar contour patterns, but the magnitudes are significantly different; the maximum deflection is increased approximately 38 percent by the presence of the perturbation.

The axial stress resultant (N_x) patterns shown in figure 8 indicate that while the maximum values without the perturbation are fairly uniformly distributed adjacent to the double-bubble tank centerline (left side of figure), the maximum values with the perturbation are concentrated away from the tank centerline at the lower boundary and near the centerline at the upper boundary. In addition, the presence of the perturbation increases the maximum value by about 40 percent.

The hoop stress resultant (N_y) contour patterns (fig. 9) show considerable differences near the double-bubble tank centerline. The presence of the perturbation with its reversal of curvature causes the large hoop stresses induced in the thickened weld area (upper boundary in the figure) to be diverted around the perturbation and even cause some hoop compression at the

centerline and also under the frame near the outer edge of the figure. While there are significant differences in the distribution of the hoop stress resultants, the maximum values are essentially the same.

The herring-bone pattern in the contours near the center of the left edge, which is particularly noticeable in figures 8b and 9b, is probably caused by the presence of high stress gradients in an area modeled with triangular elements.

The buckling mode shapes are shown in figure 10. In both cases, buckling occurred at an eigenvalue less than 1.0 indicating that the assumed prestress loading was higher than the buckling load. For comparison with the results for the cylinder, the local value of N_x in the integrally stiffened portion of the tank was used.

For the structure without the perturbation, the mode shape is fairly smooth and involves most of the area of the modeled structure. At the outer boundary (right edge), the mode shape becomes symmetric due to the assumed boundary conditions and the presence of the maximum radial displacement on this boundary indicates that an extension of the model in the circumferential direction would probably be desirable to reduce the effect of the boundary conditions on the mode shape. At buckling, the calculated value of N_x in the integrally stiffened area of the shell is 242 $kN/_m$ (1382 lb/in.). For the structure with the perturbation, the buckling mode shape shows local buckling of the tank shell between stiffeners in the integrally stiffened area. At buckling, the calculated value of N_x in the integrally stiffened area is 236 $kN/_m$ (1347 lb/in.). Local buckling probably occurs in this area because the hoop stress resultants in this area are compressive as shown in figure 9b. Therefore, the presence of the shape perturbation reduces the calculated buckling load very little (less than 3 percent), even though the maximum stress resultants are increased by amounts up to 40 percent, probably because the axial compressive loads do not change greatly in the area where buckling occurs.

In contrast to the relatively small reduction in buckling load due to the perturbation, is the reduction in the buckling load of the integrally stiffened portion of the shell when it comprises a portion of a double-bubble tank structure having variations in wall thickness and ring dimensions rather than comprising part of a uniform circular cylinder. This decrease in the value of the buckling load calculated by NASTRAN is about 22 percent.

COMPUTER TIME

Some typical NASTRAN run times on the CDC 6600 computer are shown in Table 1. The problems vary from about 300 to 900 degrees of freedom with central processor times varying from 300 seconds to 2228 seconds. A

comparison of the run times for the first three problems (NASTRAN demonstration problem and the demonstration problem with reduced thickness) shows that run times may vary considerably for what appears to be a similar problem. The large increase in run time for level 12.1.0 and $R/_t$ = 320 may be due to the selection of the range on the EIGB card which was set very low to insure that the lowest mode would be obtained. For the reduced thickness demonstration problem, level 15.1.0 shows a speed advantage of about 4 compared to level 12.1.0. A comparison of the two double-bubble runs shown indicates the significant increase in run time required to obtain several eigenvalues. The reason for calculating more than one eigenvalue is to insure that the lowest eigenvalue has been determined. For succeeding runs, the eigenvalue extraction range can usually be selected such that only one eigenvalue is required which effects a substantial reduction in run time. It is of interest to make a comparison of the NASTRAN computation times with the time required by the SALORS shell-of-revolution analysis program for finite difference buckling calculations. For an assumed axisymmetric representation of the Apollo-Saturn short stack (ref. 6) with 436 finite difference points, 209 central processor seconds were required to calculate the buckling load. In comparison, the present analysis of shells using NASTRAN with quadrilateral and triangular elements is relatively time consuming. This time consideration is offset, however, by the fact that NASTRAN may be used to analyze structures that cannot be analyzed with existing shell programs.

CONCLUSIONS

An analytical study of a two-lobed circular arc pressure vessel (double-bubble tank) with a local perturbation from the cylindrical shape has been made. From this study, it can be concluded that NASTRAN provides a good linear buckling analysis capability for structures that cannot be handled by other analysis techniques. However, at the present time, solutions are relatively expensive from a computational standpoint. Two worthwhile additions to the NASTRAN program would be the inclusion of a new beam element that adequately represents the shear transfer when modeling stiffeners on a shell, and the capability, in a rigid format, to keep certain prescribed loads constant during the eigenvalue extraction process.

REFERENCES

1. Almroth, B. O.; and Brogan, F. A.: Bifurcation Buckling as an Approximation of the Collapse Load for General Shells. AIAA J., Vol. 10, No. 4, April 1972, pp. 463-467.

2. Block, David L.; Card, Michael F.; and Mikulas, Martin M., Jr.: Buckling of Eccentrically Stiffened Orthotropic Cylinders. NASA TN D-2960, 1965.

3. NASTRAN Demonstration Problem Manual. NASA SP-224, 1970.

4. Melosh, R. J.; and Merritt, R. G.: Evaluation of Spar Matrices for Stiffness Analysis, J. of Aero./Space Science, Vol. 25, No. 9, Sept. 1958, pp. 537-543.

5. Giles, Gary L.; and Blackburn, Charles L.: Procedure for Efficient Generating, Checking, and Displaying NASTRAN Input and Output Data for Analysis of Aerospace Vehicle Structures. NASTRAN:Users' Experiences. TM X-2378, 1971, pp. 679-696.

6. Anderson, M. S.; Fulton, R. E.; Heard, W. L., Jr.; and Walz, J. E.: Stress, Buckling, and Vibration Analysis of Shells of Revolution. Computers & Structures, Vol. 1, 1971, pp. 157-192.

TABLE I

CDC 6600 COMPUTER CENTRAL PROCESSOR TIMES FOR TANK BUCKLING LOADS CALCULATION[1]

Problem	Level	Core (K OCTAL)	D.O.F.	Elements	Eigen-values	CPU Sec.
Isotropic Cylinder ($R/_t$ = 32) [2]	12.1.0	140	304	80	1	298
Isotropic Cylinder ($R/_t$ = 320) [3]	12.1.0	140	304	80	0	1127 [4]
Isotropic Cylinder ($R/_t$ = 320) [3]	15.1.0 [5]	140	304	80	1	301
5-Bay Continuous Stiffened Cylinder	12.1.0	160	880	332	1	974
Double-Bubble Tank	11.1.2	160	896	299	4	2228
Double-Bubble Tank	11.1.2	160	896	299	1	1194

1 Eigenvalue extraction method was inverse power.
2 NASTRAN demonstration axisymmetric cylinder buckling problem (ref. 3).
3 NASTRAN demonstration problem with increased $R/_t$.
4 Run exceeded time limit without determining an eigenvalue.
5 Preliminary version of level 15.1.0.

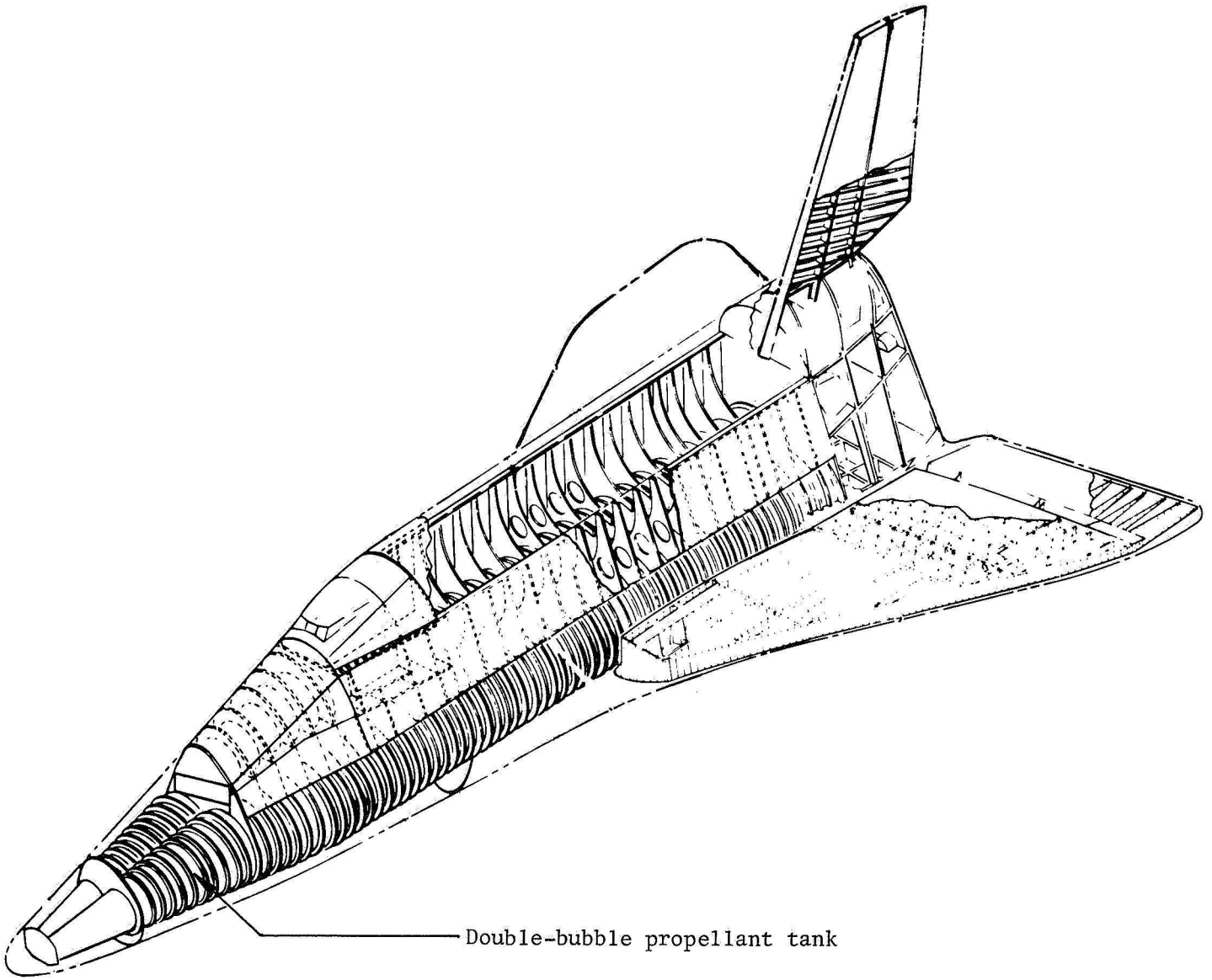

Figure 1.- Space shuttle orbiter concept with double-bubble cryogenic propellant tank.

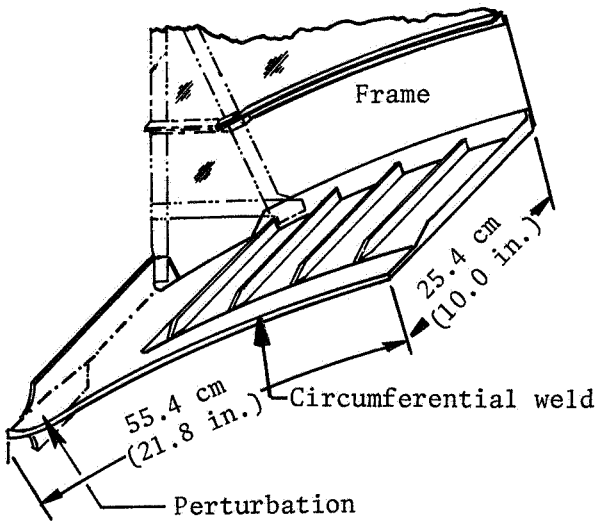

(a) Structure modeled.

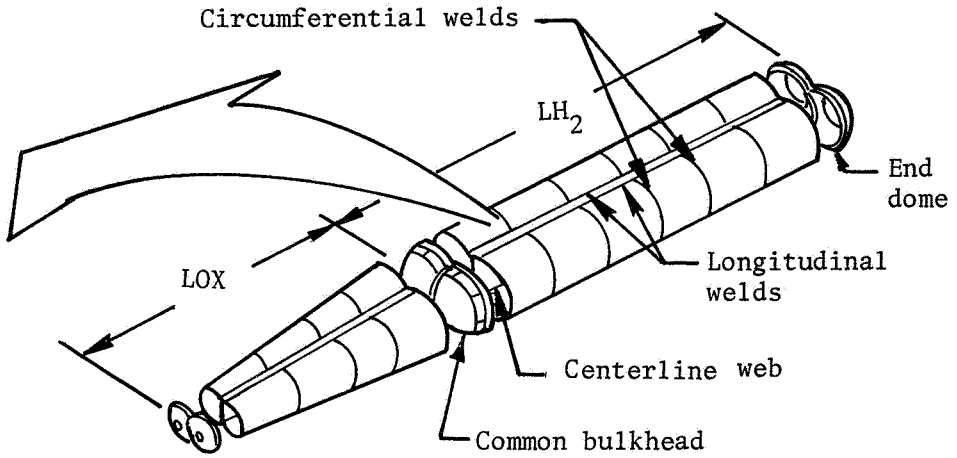

(b) Double-bubble tank.

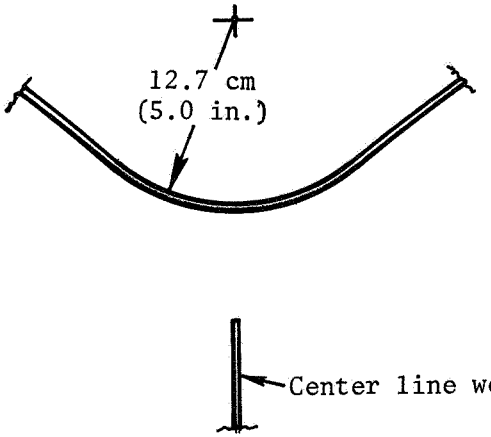

Detail A at perturbation for weld.

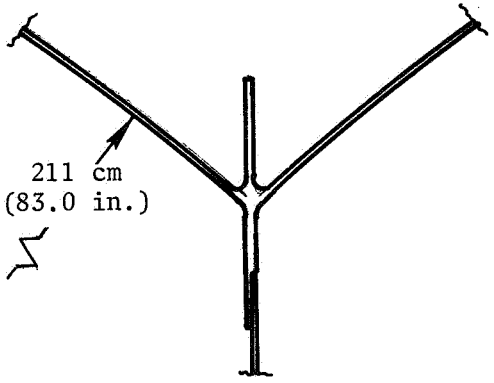

Detail A away from weld.

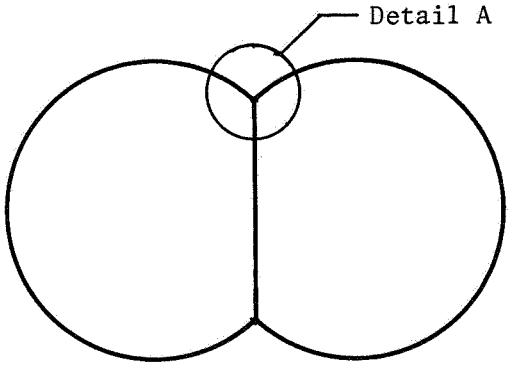

Section thru double-bubble tank.

(c) Details of shape perturbation.

Figure 2.- Double-bubble tank and shape perturbation details.

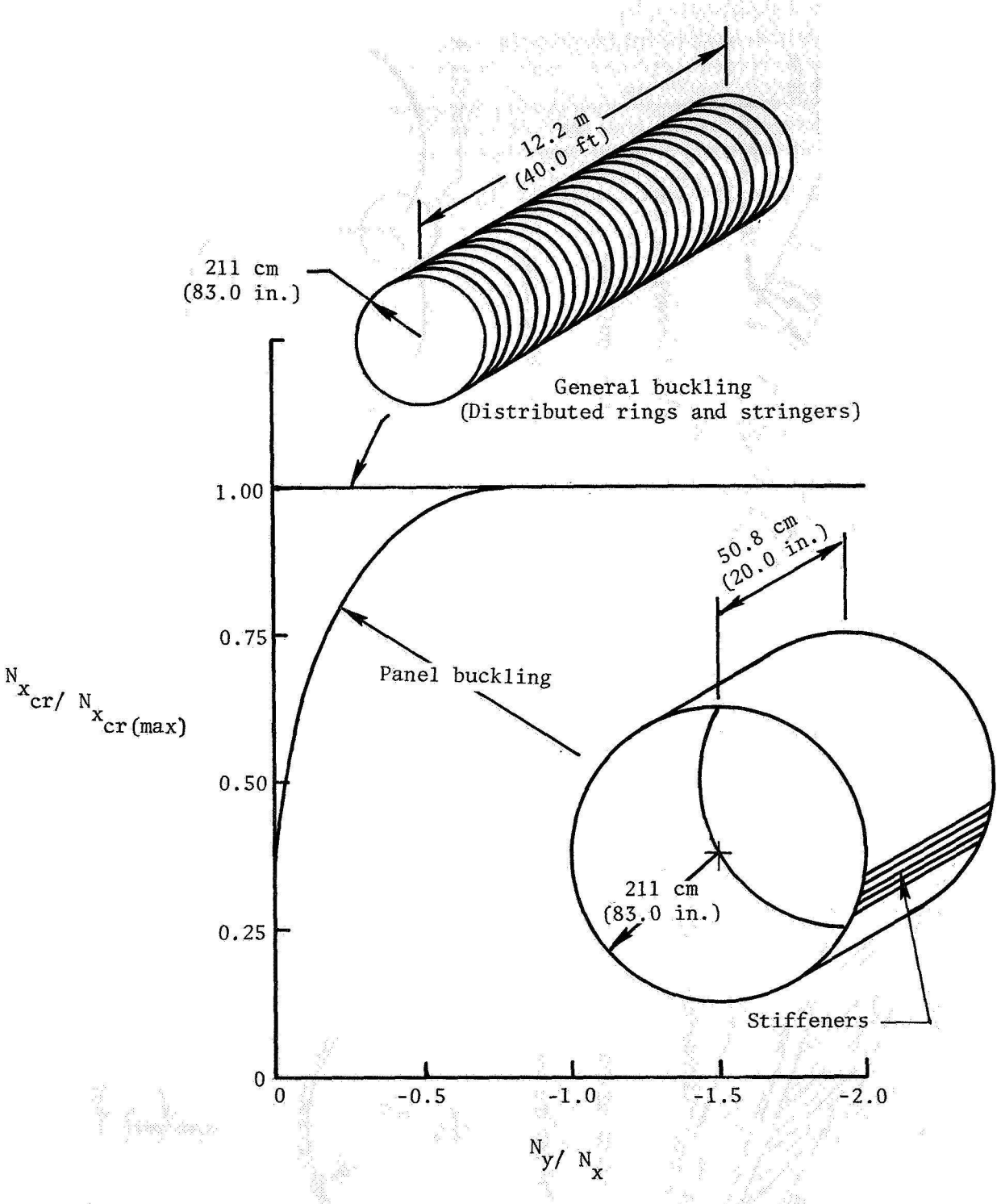

Figure 3.- Effects of stress ratio N_y/ N_x on buckling of simply-supported ring- and stringer-stiffened cylindrical shells. Results obtained from analysis of reference 2.

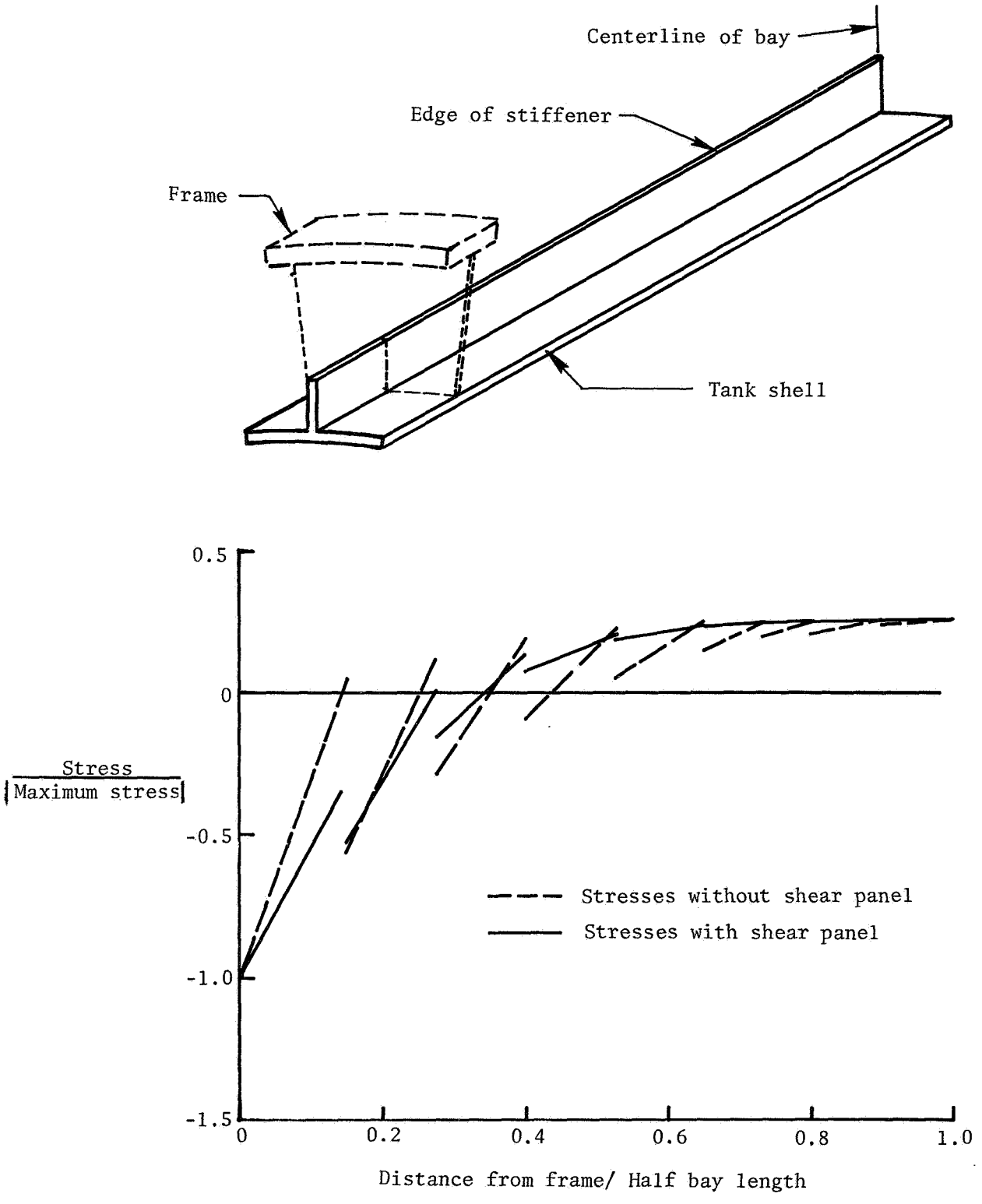

Figure 4.- Effect of stiffener modeling details on the NASTRAN calculated axial stress distribution in the edge of the stiffener.

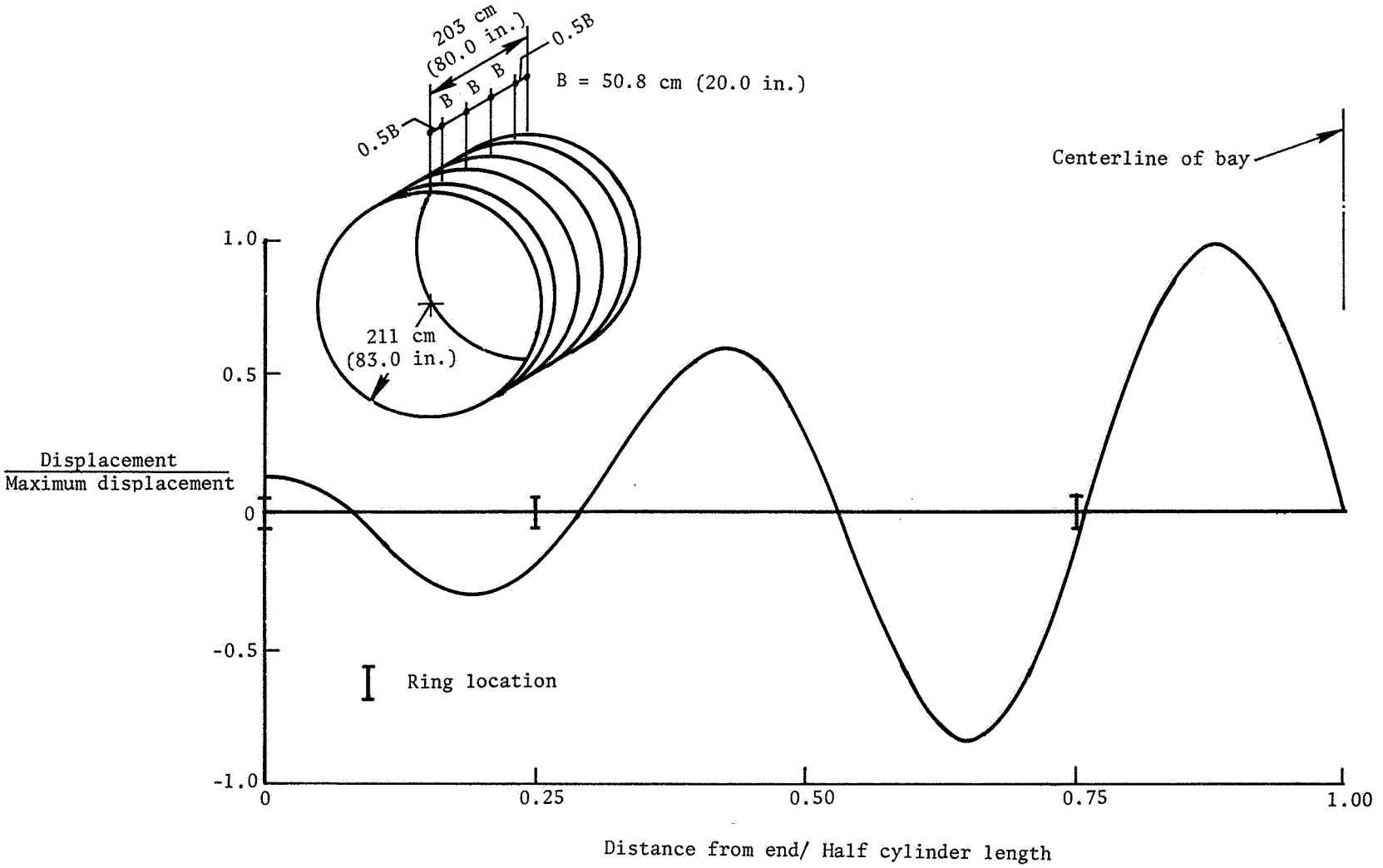

Figure 5.- Buckling mode shape of half of a multi-bay cylinder. (Mode shape antisymmetric about the centerline of bay.)

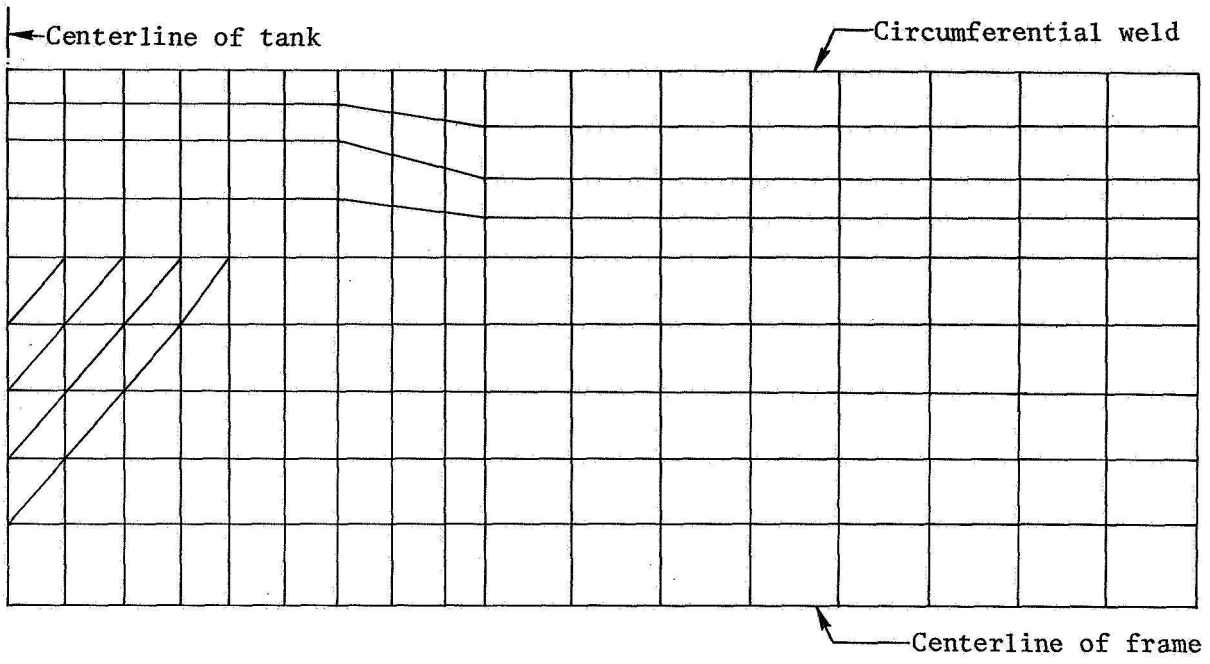

(a) Finite element model of double-bubble tank shell.

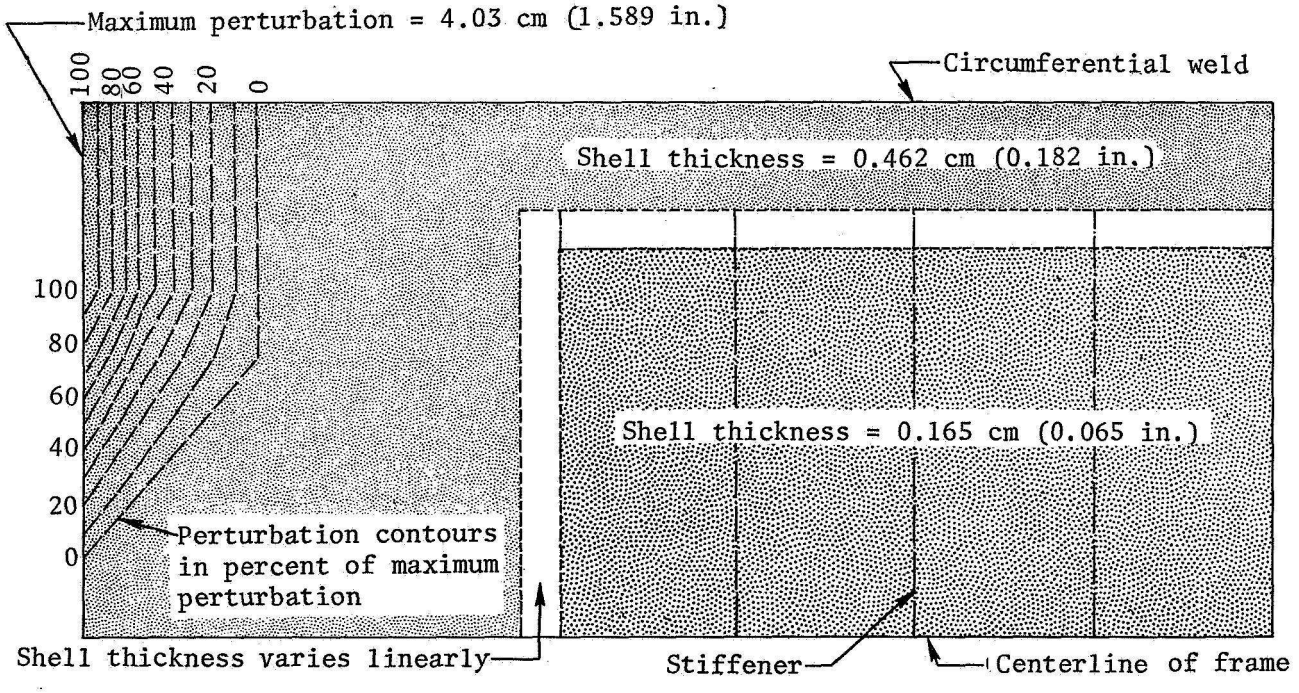

(b) Plot of shell thickness distribution and shape perturbation contours.

Figure 6.- Finite element model and shell details.

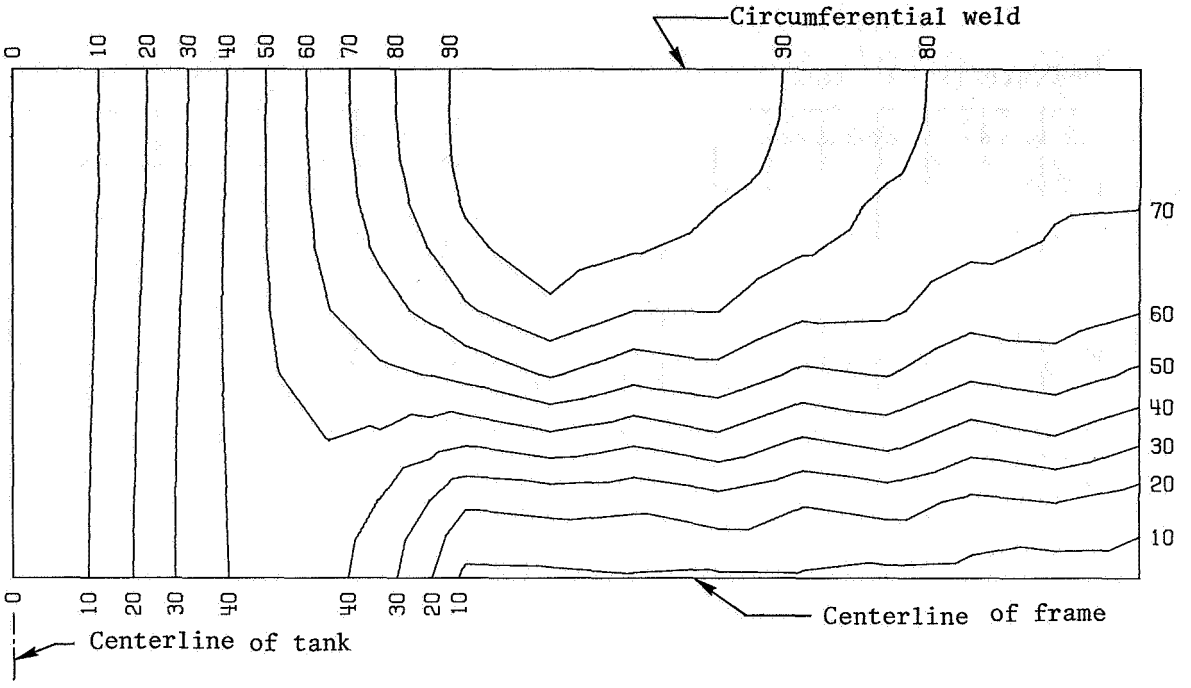

(a) Without shape perturbation. Maximum displacement = 0.620 cm (0.244 in.)

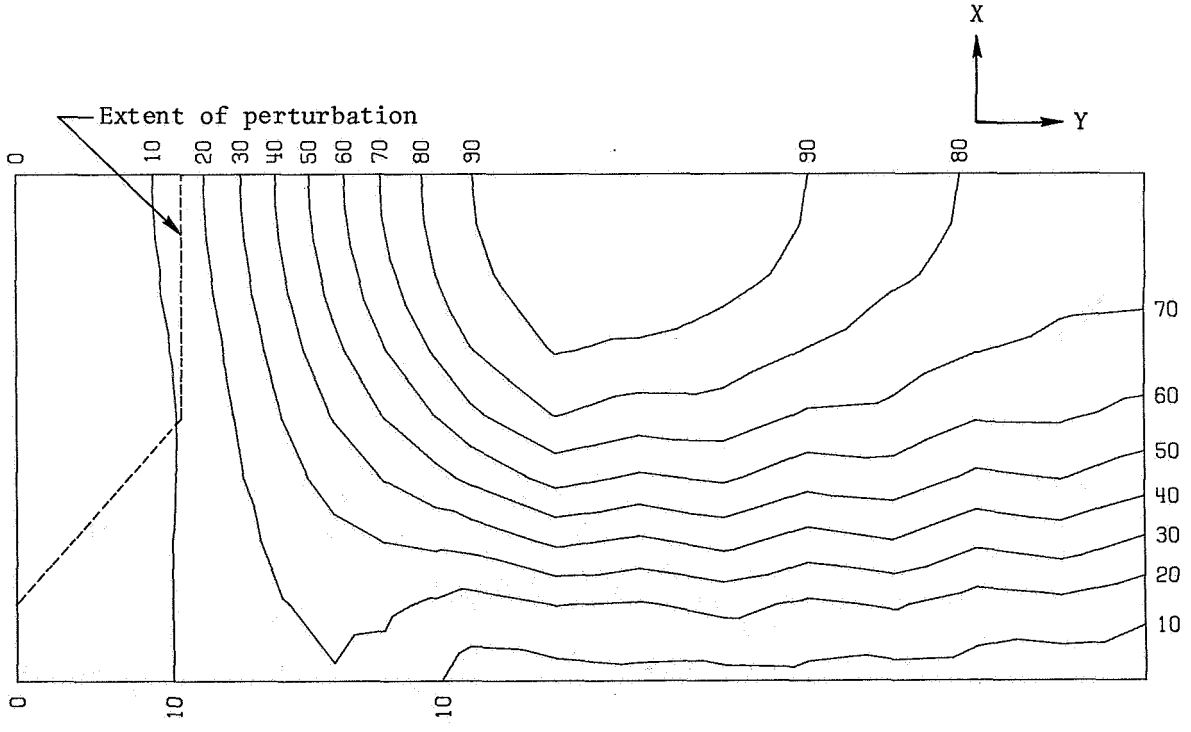

(b) With shape perturbation. Maximum displacement = 0.853 cm (0.336 in.)

Figure 7.- Contours of radial displacement under prestress loads for double-bubble tank model.

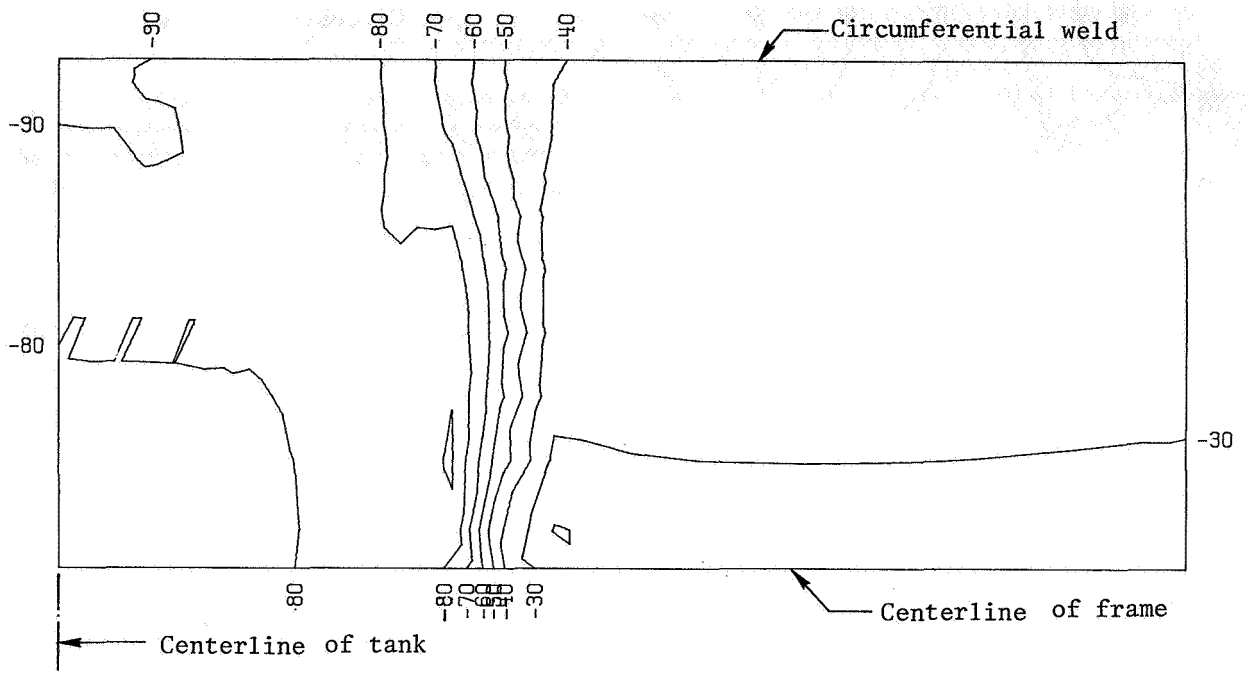

(a) Without shape perturbation. Maximum stress resultant = 775.3 $kN/_m$ (4427 lb/in.)

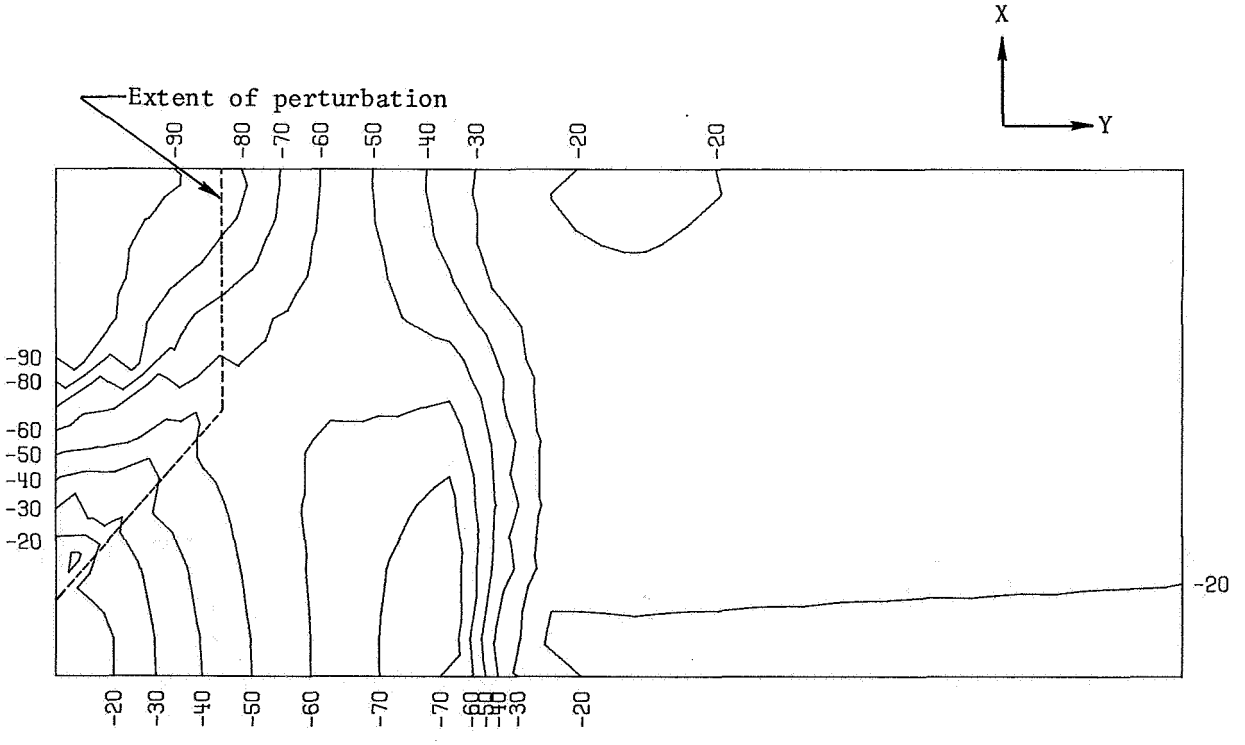

(b) With shape perturbation. Maximum stress resultant = 1089.1 $kN/_m$ (6219 lb/in.)

Figure 8.- Contours of axial stress resultant N_x for double-bubble tank model.

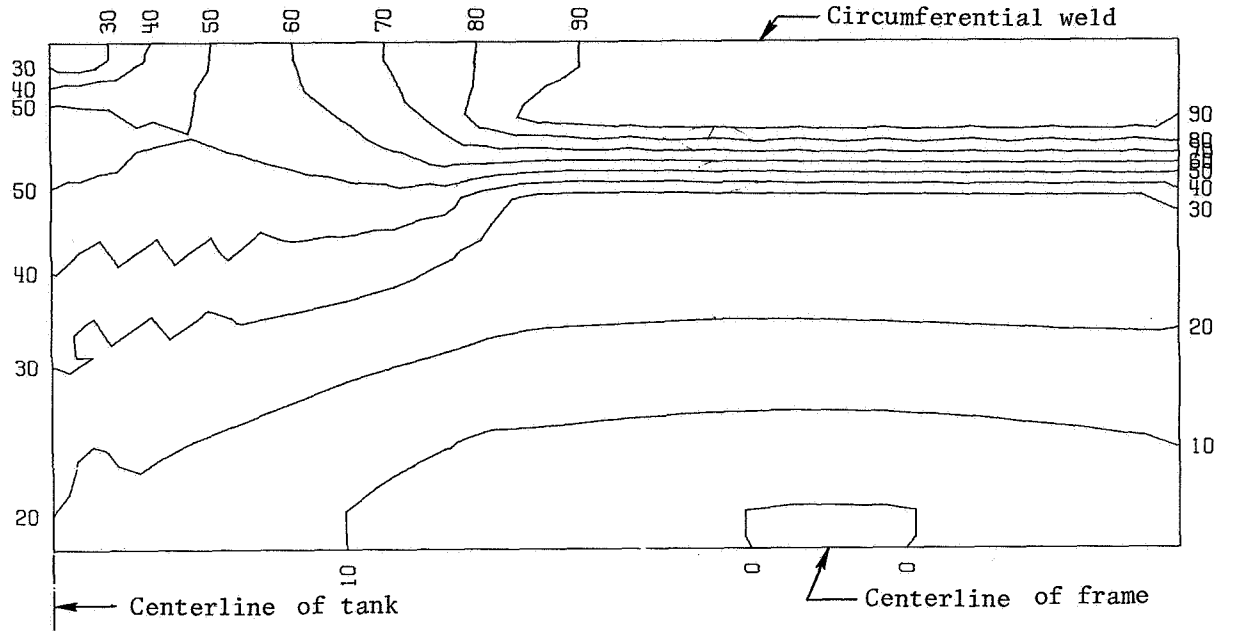

(a) Without shape perturbation. Maximum stress resultant = 716.1 kN/$_m$ (4089 lb/in.)

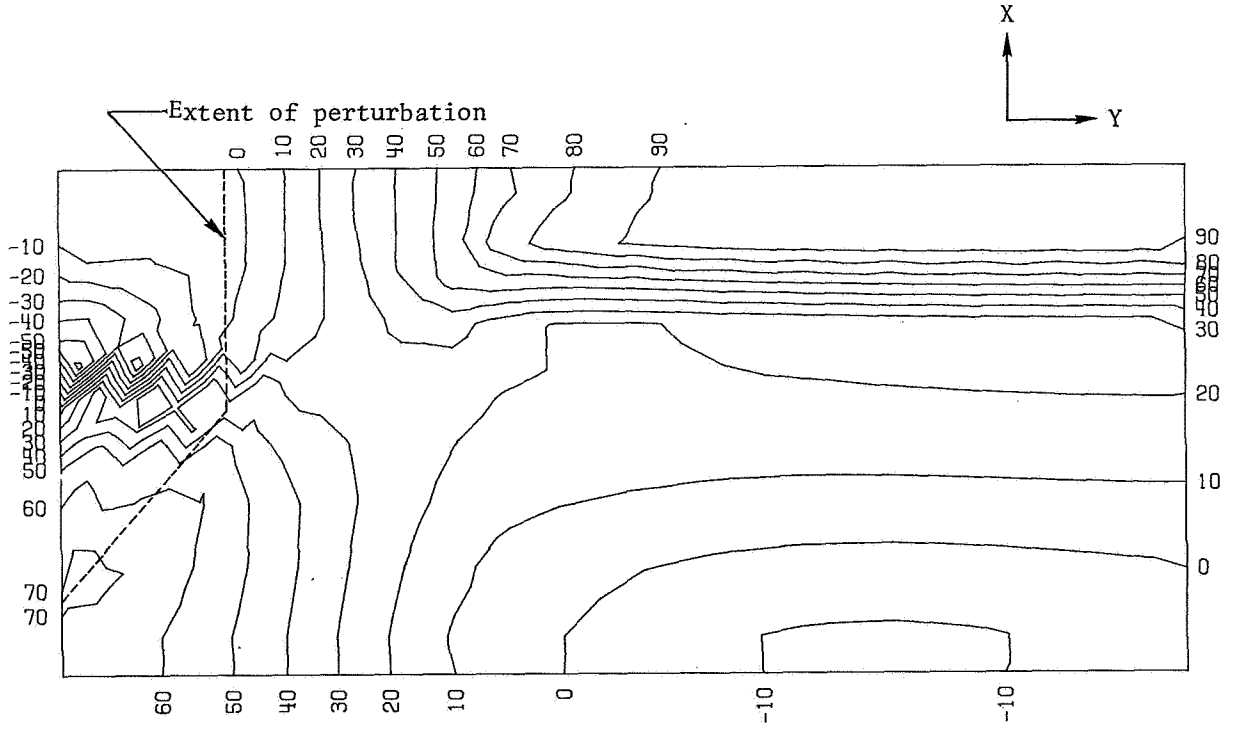

(b) With shape perturbation. Maximum stress resultant = 724.7 kN/$_m$ (4138 lb/in.)

Figure 9.- Contours of hoop stress resultant N_y for double-bubble tank model.

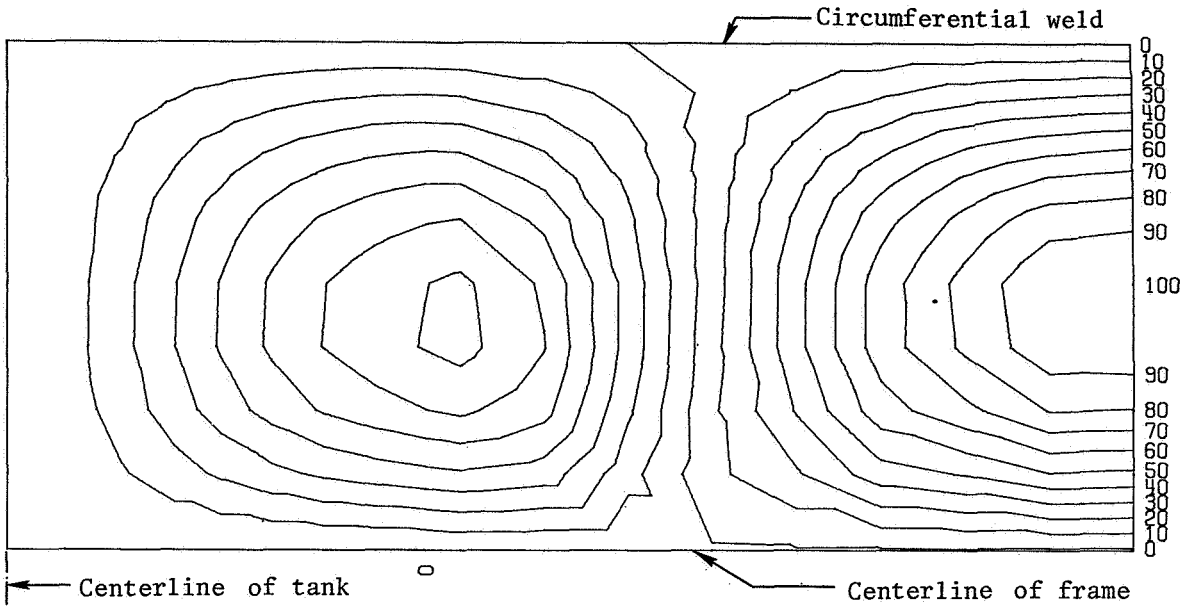

(a) Without shape perturbation.

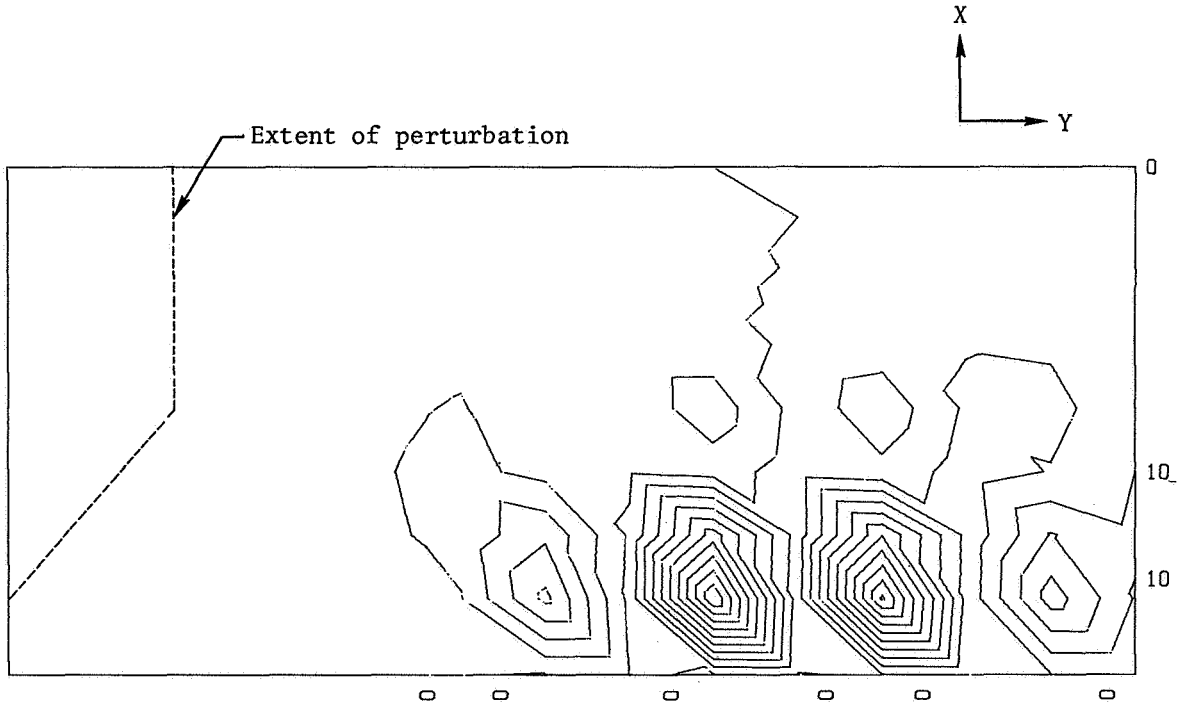

(b) With shape perturbation.

Figure 10.- Contour plot of buckling mode shape for double-bubble tank model.